Bioactive Materials 6 (2021) 1118–1129

Contents lists available at ScienceDirect

Bioactive Materials

journal homepage: www.sciencedirect.com/journal/bioactive-materials

Hydroxyapatite-modified micro/nanostructured titania surfaces with different crystalline phases for osteoblast regulation

Pinliang Jiang [a,b], Yanmei Zhang [b], Ren Hu [b], Xiankuan Wang [b], Yuekun Lai [c], Gang Rui [d], Changjian Lin [a,b,*]

[a] College of Materials, Xiamen University, Xiamen, 361005, China
[b] State Key Lab of Physical Chemistry of Solid Surfaces, and Department of Chemistry, College of Chemistry and Chemical Engineering, Xiamen University, Xiamen, 361005, China
[c] National Engineering Research Center of Chemical Fertilizer Catalyst (NERC-CFC), College of Chemical Engineering, Fuzhou University, Fuzhou, 350116, China
[d] Department of Orthopedics Surgery, The First Affiliated Hospital of Xiamen University, Xiamen, 361003, China

ARTICLE INFO

Keywords:
Micro/nanostructured surfaces
Crystalline phase
Hydroxyapatite
Cell response
Bioactivity

ABSTRACT

Surface structures and physicochemical properties critically influence osseointegration of titanium (Ti) implants. Previous studies have shown that the surface with both micro- and nanoscale roughness may provide multiple features comparable to cell dimensions and thus efficiently regulate cell-material interaction. However, less attention has been made to further optimize the physicochemical properties (e.g., crystalline phase) and to further improve the bioactivity of micro/nanostructured surfaces. Herein, micro/nanostructured titania surfaces with different crystalline phases (amorphous, anatase and anatase/rutile) were prepared and hydroxyapatite (HA) nanorods were deposited onto the as-prepared surfaces by a spin-assisted layer-by-layer assembly method without greatly altering the initial multi-scale morphology and wettability. The effects of crystalline phase, chemical composition and wettability on osteoblast response were investigated. It is noted that all the micro/nanostructured surfaces with/without HA modification presented superamphiphilic. The activities of MC3T3-E1 cells suggested that the proliferation trend on the micro/nanostructured surfaces was greatly influenced by different crystalline phases, and the highest proliferation rate was obtained on the anatase/rutile surface, followed by the anatase; but the cell differentiation and extracellular matrix mineralization were almost the same among them. After ultrathin HA modification on the micro/nanostructured surfaces with different crystalline phases, it exhibited similar proliferation trend as the original surfaces; however, the cell differentiation and extracellular matrix mineralization were significantly improved. The results indicate that the introduction of ultrathin HA to the micro/nanostructured surfaces with optimized crystalline phase benefits cell proliferation, differentiation and maturation, which suggests a favorable biomimetic microenvironment and provides the potential for enhanced implant osseointegration in vivo.

1. Introduction

Titanium and its alloys have been commonly used for hard tissue replacements including dental implants, artificial bones and joints, owing to their favorable biocompatibility, suitable mechanical properties and high corrosion resistance [1,2]. However, the mechanically polished Ti surface is bioinert and it is normally encapsulated by fibrous tissues, leading to implantation failure [1,2]. As a consequence, it is necessary to modify the surface physicochemical properties of Ti implants, such as morphology, composition and wettability to enable favorable bioactivity and biocompatibility [1,2]. Natural bone is a hierarchical hybrid organization composed of macro-, micro- and nano-scale structures, and such a hierarchically assembled tissue is to realize diverse mechanical, biological and chemical roles [3]. From the viewpoint of bionics, a multi-level structure on implants comprised both micro- and nano-scale features tends to benefit the expressions of cell functions because cell-material interaction occurs across multiple length scales during bone remodeling [3]. Several works have intended to

* Corresponding author. State Key Lab of Physical Chemistry of Solid Surfaces, and College of Chemistry and Chemical Engineering, Xiamen University, Xiamen, 361005, China.
E-mail address: cjlin@xmu.edu.cn (C. Lin).

https://doi.org/10.1016/j.bioactmat.2020.10.006
Received 29 July 2020; Received in revised form 21 September 2020; Accepted 8 October 2020

examine the influence of micro/nanostructures on osteoblast or stem cell response [4–9], but in some cases, incompatible results of specific cell functions were obtained [5–8]. For instance, Zhao et al. prepared a micro/nano-textured surface composed of micropitted and nanotubular TiO_2 structures via acid etching and anodization, and it is observed that the proliferation, ALP activity and extracellular matrix mineralization of primary rat calvarial osteoblasts on certain micro/nano-textured surfaces were somewhat maintained or promoted when compared to those on smooth surfaces [5]. Gittens et al. used a simple oxidation treatment to generate nanoscale protuberances on micro-/submicro-scale roughness, and noted that the expression and secretion of osteocalcin, osteoprotegerin, and vascular endothelial growth factor of MG63 cells were greatly enhanced compared with those on smooth surfaces, but the proliferation was obviously reduced [6]. From the comparison of their reports, the different cell activities are closely related to various factors, such as surface morphology, wettability, crystalline phase of TiO_2 as well as cell origins. A number of studies have concerned the construction of specific surface morphology and wettability of micro/nanostructures over the recent years [4–7,10], however, few works have addressed the effect of oxide crystalline phase of micro/nanostructured surfaces on cell response up to now.

Previous studies have indicated that the crystalline phase of TiO_2 plays a vital role in regulating cell activities [11–15]. Oh et al. observed that the proliferation and ALP activity of MC3T3-E1 cells were accelerated on TiO_2 nanotubes with anatase phase compared with them on amorphous nanotubes [11]. Yu et al. reported that the crystallized TiO_2 nanotubes (anatase or anatase/rutile) displayed significantly higher proliferation and mineralization of MC3T3-E1 cells than amorphous nanotubes, and notably, the anatase/rutile presented slightly better performance in promoting cell proliferation and mineralization than the anatase [12]. He et al. prepared TiO_2 films with three different crystalline phases (amorphous, anatase and rutile) via magnetron sputtering, and showed that the adhesion, proliferation and ALP activity of primary rat osteoblasts were obviously improved on the anatase compared to them on the amorphous and rutile, but there was no difference in biological effects between the amorphous and rutile [13]. According to the above reports, it is clear that the crystalline phase of TiO_2 strongly influences the cell activities on the surfaces with similar morphology and roughness, even though the present results are controversial and inconsistent. Therefore, it is necessary to elucidate the relationship between crystalline phase and osteoblast response, which would help optimize the bioactivity of micro/nanostructured surfaces.

HA is proved to be a kind of bioactive ceramics and it possesses osteoconductivity as well as intrinsic osteoinductive potential [16–19]. It is noted that HA is able to support osteoblast adhesion, differentiation in vitro and directly bond to bone without forming an intermediate fibrous tissue layer at the material-bone interface in vivo [20]. Although the precise mechanism of stimulation is still unclear, the bioactivity of HA is probably associated with the dissolution, precipitation and ion exchange process occurred under the physiological conditions [16,20]. A number of works have focused on preparations of HA or HA-contained coatings on Ti surfaces, and their results presented that HA-deposited Ti surfaces can markedly improve cell or tissue activity [19,21–23]. Furthermore, the HA-modified Ti implants mostly via thermal spraying have achieved clinical applications in the last decades [24,25], however, there are some disadvantages that include thermal decomposition of the HA powders during spraying, the inability to regulate pore sizes and porosity in hierarchical dimensions, and the difficulty to prepare coatings of less than ~20 μm thickness [25]. Hence, it is still needed to develop some new or combined methods to properly apply HA as a coating or as a component to tailor Ti surface concerning the osseointegration capability. Herein, the hypothesis is that the combination of nanoscale HA with hierarchical hybrid TiO_2 of crystallized layer on Ti substrate may be an alternative to better mimic the structure and composition of natural bone, and to satisfy the requirements of remodeling processes where osteoblast occupies the hierarchical structural complexity to secrete and deposit unmineralized bone matrix [26]. To our knowledge, the combined effects of ultrathin film of nanoscale HA and micro/nanostructured surfaces on osteoblast response is rarely reported yet.

In this study, the relationship between crystalline phase of micro/nanostructured surfaces and osteoblast activities was systematically investigated. The surface structure and properties were optimized to favor the multiple cell functions of osteoblasts. Additionally, in order to endow the Ti surfaces with promoted bioactivity, an ultrathin film of HA nanorods were deposited onto the micro/nanostructured surfaces with different crystalline phases, but some certain physicochemical properties (e.g., morphology and wettability) of the initial micro/nanostructured surfaces were well retained, whose influence on cell response was elucidated as well. The HA-modified micro/nanostructured surfaces with proper crystalline phase are expected to provide a biomimetic microenvironment for cell or tissue ingrowth and thus improve the bioactivity and biocompatibility of Ti implants.

2. Materials and methods

2.1. Preparation of samples

Pure titanium discs (15 mm in diameter and 2 mm in thickness) were carefully polished by SiC sandpapers, and then followed by ultrasonic cleaning with acetone, anhydrous ethanol and distilled water for 10 min, respectively. To construct a micropitted/nanospongelike structured surface, the Ti substrates were immersed in a mixed acid solution composed of 48% H_2SO_4 and 18% HCl for 1 h at 75 °C, and then electrochemically anodized in an ethylene glycol solution containing 0.3 wt % NH_4F and 0.2 wt% H_2O_2 at 50 V for 30 min (designated as MS). The different crystalline phases of the micropitted/nanospongelike structured surface were obtained by annealing the samples in air at 450 °C, 550 °C or 650 °C for 2 h (designated as MS-450, MS-550 or MS-650, respectively).

The deposition of calcium phosphate (CaP) onto the above constructed surfaces was carried out by a spin-assisted layer-by-layer assembly technique (designated as MS-HA, MS-450-HA and MS-550-HA). A droplet (120 μL) of saturated $Ca(OH)_2$ solution was first dropped onto the samples and rotated at a speed of 3000 rpm for 40 s. Then, a droplet (120 μL) of 0.02 M $(NH_4)_2HPO_4$ solution was dropped onto the precoated samples and rotated in the same manner. The alternating spin-assisted assembly procedure was repeated until 20 cycles. Finally, the samples were rinsed by distilled water and air-dried.

2.2. Surface characterization

The surface morphology of the prepared samples was observed using a field-emission scanning electron microscope (FESEM; Hitachi S4800, Japan). The crystalline phase of the samples was evaluated using an X-ray diffractometer (XRD; PANalytical X'pert PRO, Holand) with a Cu-K_α radiation source at 40 kV and 30 mA. The crystallinity (X_c) of HA was calculated according to the following equation: $X_c = 1 - (V_{112/300}/I_{300})$, where $V_{112/300}$ represents the intensity of the hollow between peak (112) and peak (300) diffraction peaks, and I_{300} represents the intensity of the peak (300) [27]. Surface atomic concentration was obtained using an X-ray photoelectron spectroscopy (PHI Quantum 2000 XPS, USA) with a monochromatic Al-K_α source and a charge neutralizer. The binding energies of the elements were calibrated according to the binding energy of carbon ($C_{1s} = 285.0$ eV). Surface roughness (R_a) at the microscale features was determined by using a three-dimensional laser scanning confocal microscope (LSCM, VK-X100/X200, Keyence, Japan).

2.3. Contact angle measurement

Contact angles of the prepared samples were measured using a contact angle measuring system (Kruss DSA100, Germany). The liquid

droplet of distilled water, ethylene glycol, diiodomethane or n-hexadecane, with a volume of 3 μL, was dropped onto each substrate and then the captured image was analyzed with the image analysis software to determine the contact angle of air-liquid-substrate interface. Three samples were measured for each prepared group.

2.4. Calcium ion release

To determine Ca^{2+} ion release, the HA-modified sample was immersed in 2.5 mL PBS and placed in cell culture incubator at 37 °C. At the predetermined time points, the supernatant was totally collected and stored at 4 °C. The volume of collected supernatant was diluted and the concentration of Ca^{2+} ion was detected by ICP-OES spectrometer (iCAP 7000, Thermo Scientific, US).

2.5. Protein adsorption assay

A drop size of 1 mL α-MEM (Minimum Essential Medium Eagle, alpha modification) supplemented with 10% fetal bovine serum (FBS) was added onto each titanium sample. After incubation for 2 h at 37 °C, the samples were transferred to another 24-well plate and washed with PBS thrice. Afterward, the adsorbed protein on the sample was detached by adding 500 μL of 1% sodium dodecyl sulfate (SDS) and the protein amount was quantified using a BCA protein assay kit (Applygen Technologies Inc, China).

2.6. In vitro cell culture

MC3T3-E1 pre-osteoblastic cells were used to compare cell response to the different substrates. The cells were cultured in α-MEM containing 10% fetal bovine serum (FBS), 100 units/mL penicillin and 100 μg/mL streptomycin, and incubated under a humidified atmosphere with 5% CO_2 at 37 °C. When nearly reaching 90% of confluence, the cells were harvested with 0.25% trypsin for subsequent assays. After sterilized by 75% alcohol for 1 h, the samples were put into a 24-well plate and covered by cell suspension with a density of 2×10^4 cells/well. To evaluate cell adhesion, cytotoxicity, morphology and proliferation, cells were cultured in a growth medium; while for the osteoblast differentiation assays, the cells were cultured in a growth medium supplemented with 50 μg/mL of L-ascorbic acid and 10 mM of β-glycerophosphate sodium. The culture medium was replaced every other day.

2.7. Lactate dehydrogenase activity assay

The lactate dehydrogenase (LDH) activity was measured to show the potential cytotoxicity of the samples. After incubation for 24 h, the culture medium of each sample was collected and centrifuged. The supernatant was analyzed to determine the amount of lactate dehydrogenase leakage of MC3T3-E1 cells into the culture medium using an LDH kit (Nanjing Jiancheng Bioengineering Institute, China) according to the manufacturer's instructions.

2.8. Cell morphology

After 1 day and 14 days of incubation, the cells grown on the samples were rinsed twice with phosphate buffer saline (PBS), fixed with 2.5% glutaraldehyde at 4 °C for 2 h and dehydrated in a graded series of ethanol (30%, 50%, 70%, 90% and 100%). After that, the samples were dried in a freeze dryer (Eyela FDU-1200, Tokyo Rikakikai, Japan) and then sputtered with platinum for SEM observation. In addition, the cell morphology was also observed after Calcein-AM (Sigma) staining, under a fluorescence microscope (TCS SP8, Leica, Germany).

2.9. Cell proliferation

Cell proliferation was evaluated by MTT assay. After 1, 4 and 7 days of cell culture, 200 μL of 5 mg/mL MTT solution was added to each sample and incubated at 37 °C to form insoluble formazan crystals. Then the MTT-containing medium was removed and replaced with 1 mL of dimethyl sulfoxide to dissolve formazan. The optical density (OD) at 490 nm was measured by using a microplate reader (Tecan Infinite M200, Switzerland).

2.10. Alkaline phosphatase activity assay

Alkaline phosphatase (ALP) activity was determined to evaluate the early-stage differentiation of MC3T3-E1 cells. After incubation for 7 and 14 days, the cells on the samples were rinsed thrice with PBS and lysed with 500 μL of 0.2% Triton X-100. The absorbance at 520 nm was measured using an ALP assay kit (Nanjing Jiancheng Bioengineering Institute, China) according to the manufacturer's instructions. Intracellular protein content was determined by BCA protein assay and the ALP activity was normalized to it.

2.11. Collagen secretion assay

Collagen secretion from the MC3T3-E1 cells was evaluated by Sirius Red staining. After incubation for 7 and 14 days, cells on the samples were fixed with 4% paraformaldehyde for 1 h and stained with 0.1% Sirius Red in saturated picric acid for 18 h. Afterward, the stained samples were washed with 0.1 M acetic acid, dried in air and imaged under an optical microscope. For quantitative analysis, each stained sample was eluted in 1 mL of mixed solution composed of 0.2 M NaOH and methanol (1:1), and the absorbance at 528 nm was measured using a microplate reader.

2.12. Extracellular matrix mineralization assay

The matrix mineralization of the cells was analyzed by SEM observation and calcium content assay. After incubation for 14 days, cells on the samples were fixed with 2.5% glutaraldehyde, dehydrated in a graded series of ethanol and freeze-dried for SEM observation. For quantitative analysis, the samples were immersed in 1 M acetic acid and gently shaken overnight. Afterward, the solution was collected and determined for calcium content by a calcium assay kit (Nanjing Jiancheng Bioengineering Institute, China) according to the manufacturer's instructions. The absorbance at 610 nm was measured using a microplate reader. Additionally, the calcium content of the HA on the MS-HA, MS-450-HA and MS-550-HA was quantified as well to avoid the interference.

2.13. Statistical analysis

The data were expressed as mean values ± standard deviations (SD) and compared via one-way variance analysis (ANOVA) with SPSS 11.0 software. A value of $p < 0.05$ was considered to be statistically significant.

3. Results and discussion

3.1. Morphology and composition analysis

As shown in Fig. 1, a hierarchical hybrid structure composed of micropitted and nanospongelike TiO_2 was constructed on Ti surface via a combined treatment of dual-acid etching and electrochemical anodization. In order to obtain different crystalline phases of TiO_2, the Ti substrates with micro/nanostructured surfaces were annealed at different temperatures. It is noteworthy that the micropitted features were well preserved without discernible changes at different annealing temperatures, whose pore size fell in the range of 1–12 μm (with similar mean values), but the nanospongelike structures were moderately altered, even the pore sizes similarly ranged between 15 nm and 200 nm,

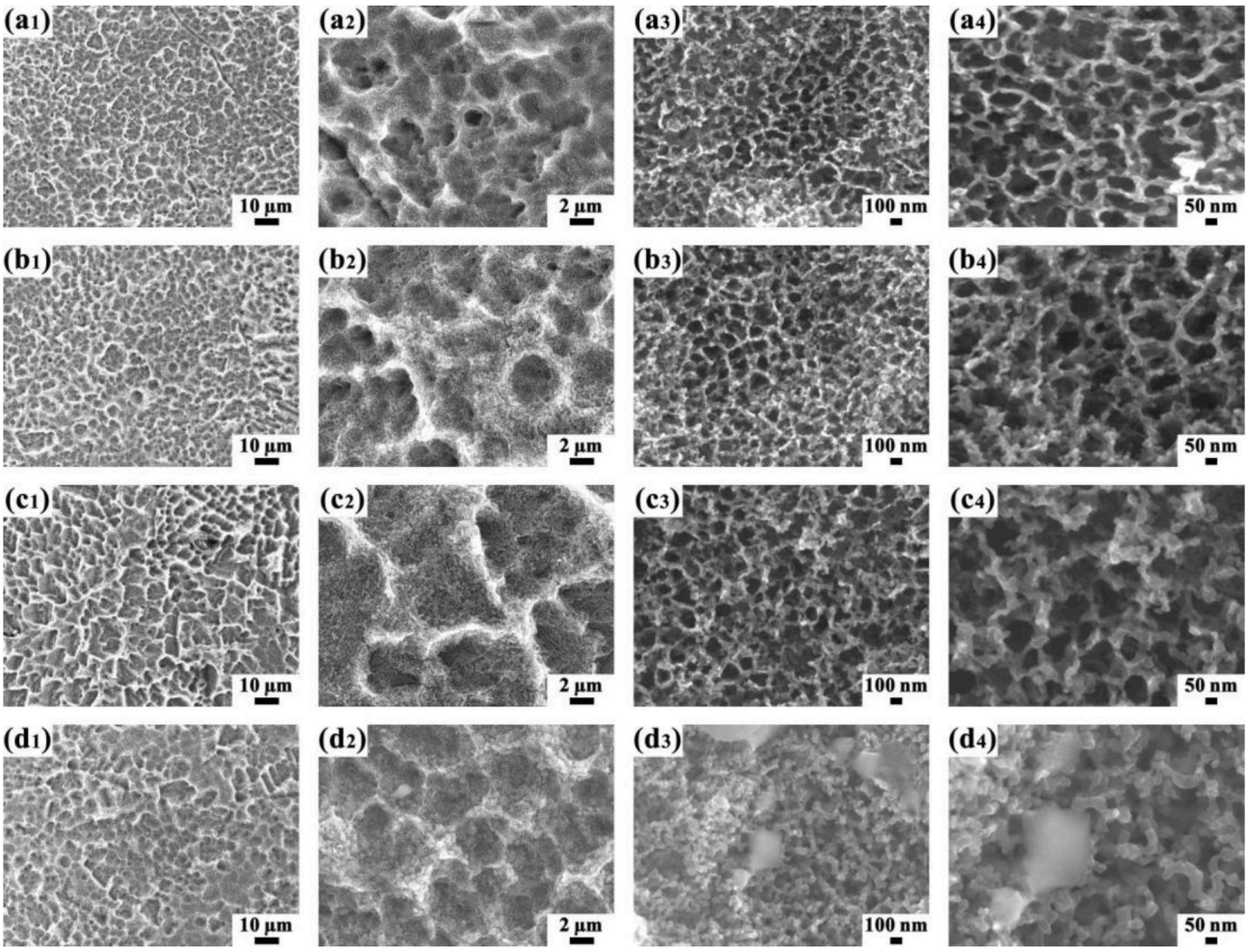

Fig. 1. SEM images of different Ti samples after calcination at different temperatures: (a) MS, (b) MS-450, (c) MS-550 and (d) MS-650. Parts a_2−d_2 are high-magnification images of the samples in a_1–d_1, respectively, parts a_3−d_3 are high-magnification images of the samples in parts a_2–d_2, respectively, and parts a_4−d_4 are high-magnification images of the samples in a_3–d_3, respectively.

as shown in Fig. S1 and Table S1. Notably, the nanoporous wall on MS was smooth, with a wall thickness of 20.04 ± 5.48 nm, however, after annealed at 450 °C, the wall on MS-450 became slightly rough and small protrusions appeared on it, with a wall thickness slightly increased to 21.86 ± 4.08 nm. After annealed at 550 °C, the protrusions on the wall grew larger and the wall was thickened to 25.26 ± 5.23 nm. Following annealed at 650 °C, besides the wall was further thickened to 29.27 ± 5.39 nm, parts of the nanospongelike structure collapsed and some protrusions coalesced into coarser and larger grains over the nanoscale structure. The changes in surface morphology of nanospongelike structure were due to the fact that the calcination enabled the nanospongelike TiO_2 to nucleate, emerge through porous structure when the temperature increased [28]. In order to retain the micro/nanostructured surface well, in the following parts, we used the samples calcined at 450 °C or 550 °C to compare the relationship between surface physicochemical properties (e.g., crystalline phase and wettability) and cell response.

The ultrathin film of CaP nanorods were deposited onto the micro/nanostructured surface via a spin-assisted layer-by-layer assembly method. As shown in Fig. S2A, small CaP grains appeared on the nanoporous structure when the substrates were exposed to 5 cycles of assembly. With the number of cycles increased to 10, the CaP grains were augmented and a portion of them appeared needle-like. After 15 cycles of assembly, the CaP compounds continued to deposit and turned into a nanorod-like shape. After 20 cycles, the CaP nanorods became slightly coalesced and elongated.

To confirm the chemical and structural properties, the CaP deposits were scraped off for XRD and FTIR measurements. It is clear that the diffraction of CaP deposits was comparable to the reference data of HA (JCPDS 86–0740) with a degree of crystallinity of 35%, and no secondary phases were measured, as shown in Fig. S2B. From the FTIR spectrum (Fig. S2C), the CaP deposits comprised carbonated HA. Besides the bands (1641 cm^{-1} and 3405 cm^{-1}) of incorporated water molecules, the bands at 633 cm^{-1} and 3570 cm^{-1} were typical stretching and librational modes of –OH groups in HA [29]. The bands at 470 cm^{-1} was associated with the bending vibration (ν_2) of PO_4^{3-} groups [29,30]. The bands at 564 cm^{-1} and 603 cm^{-1} reflected the bending vibrations (ν_4) of PO_4^{3-} groups [29,30]. The bands at 1033 cm^{-1} and 1091 cm^{-1} were assigned to antisymmetric stretching vibrations (ν_3) of PO_4^{3-} groups [29]. The band at 962 cm^{-1} was derived from symmetric stretching (ν_1) of PO_4^{3-} groups [30]. Additionally, the bands at 879 cm^{-1} and 1454 cm^{-1} were attributed to the vibrations (ν_2 and ν_3) of CO_3^{2-} groups [29, 30], indicating that the CaP deposits were carbonated HA. Hence, the results of XRD and FTIR measurements confirm that the CaP nanorods are composed of carbonated HA.

In order to improve the bioactivity of different crystalline phases, the HA nanorods were prepared on the MS, MS-450 and MS-550 samples via 20 cycles of deposition to obtain the HA-modified micro/nanostructured surfaces, namely MS-HA, MS-450-HA and MS-550-HA, respectively. Fig. 2 shows the representative morphology of the different samples with/without HA. It is evident that the HA nanorods appeared perpendicular to the surface and moderately changed the nanoporous

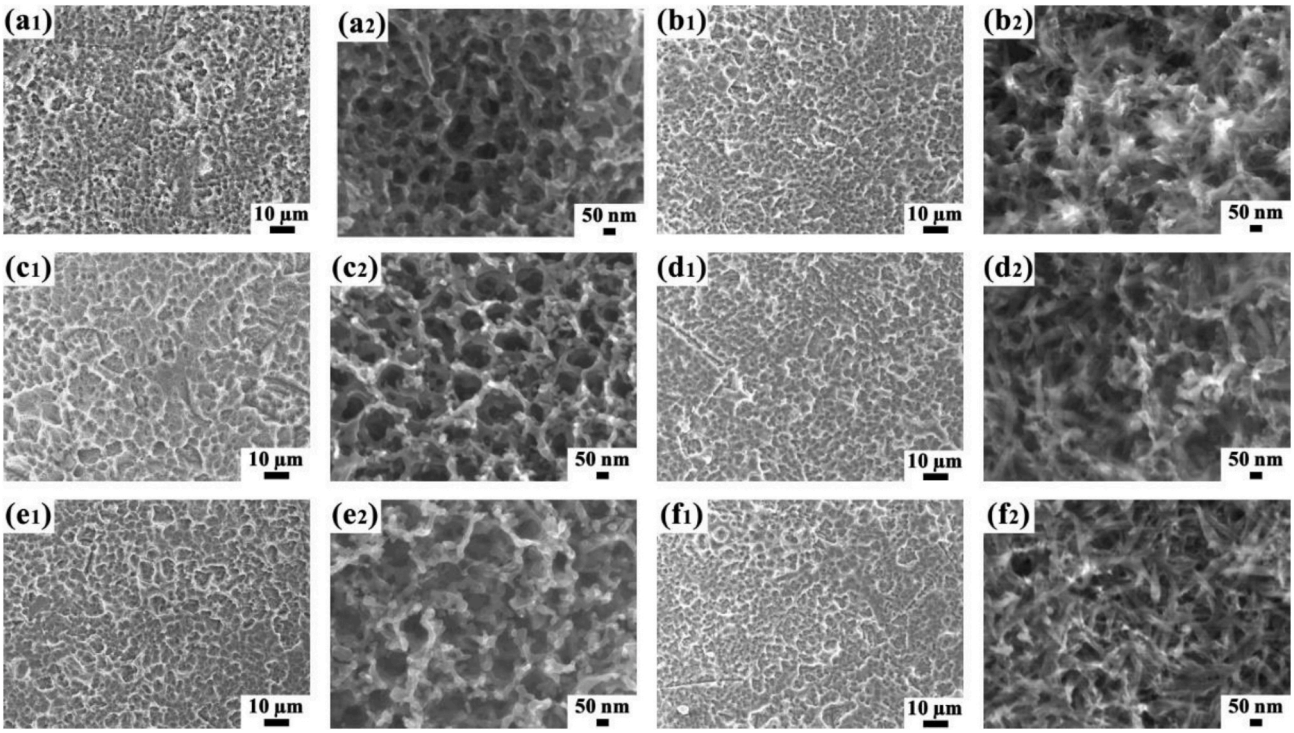

Fig. 2. SEM images of different Ti samples: (a) MS, (b) MS-HA, (c) MS-450, (d) MS-450-HA, (e) MS-550 and (f) MS-550-HA. Parts a_2–f_2 are high-magnification images of the samples in a_1–f_1, respectively.

structure; however, the surface morphology at the microscale features was well preserved, with an average value of surface roughness (R_a) ranging from 2.16 ± 0.29 μm to 2.39 ± 0.36 μm for the different samples (Table 1).

The XRD analysis was used to identify the crystalline phases and chemical composition of the prepared samples with/without HA deposition. As shown in Fig. 3A, all the samples displayed typical α-Ti diffraction peaks. For the MS and MS-HA, they yielded the diffraction peaks of TiH_2 (41°, 59.3°), which was resulted from the fact that the acid etching caused the evolved hydrogen to react with the Ti [31]. However, after annealing at 450 °C or 550 °C, the TiH_2 was decomposed by heat treatment. For MS-450 and MS-450-HA, the diffraction peaks of anatase (25.2°, 48°) were detected. Besides the diffraction peaks of anatase, additional diffraction peaks of rutile (27.6°) were observed on MS-550 and MS-550-HA. It is noteworthy that MS-HA, MS-450-HA and MS-550-HA did not display the characteristic peaks of HA, because the amount of the HA nanorods on each sample was not enough to induce the diffraction.

Raman spectroscopy was used to characterize chemical composition of the prepared samples as well. As shown in Fig. 3B, C, MS did not show any active Raman modes because of the amorphous nature of TiO_2. In contrast, both of MS-450 and MS-550 samples displayed five active Raman modes of anatase, namely three E_g modes at 144 cm^{-1}, 196 cm^{-1} and 639 cm^{-1}, an overlapping A_{1g}/B_{1g} doublet at 513/519 cm^{-1} as well as a B_{1g} mode at 397 cm^{-1} [32]. Besides the Raman modes of anatase, MS-550 and MS-550-HA also exhibited a weak Raman mode of rutile at 447 cm^{-1} [32], indicating that TiO_2 on the surfaces were composed of mixed phases, mainly anatase and rutile. After HA modification, MS-HA, MS-450-HA and MS-550-HA yielded an additional Raman mode at 960 cm^{-1}, which was assigned to the symmetric stretching of PO_4^{3-} groups (ν_1) in HA [33]. In short, the results of Raman spectroscopy are consistent with the characterization of XRD and FTIR measurements.

The chemical composition of the prepared surfaces was characterized by XPS analysis. The XPS spectra and the corresponding element concentrations were listed in Fig. S3 and Table 2, respectively. As shown in Fig. S3, all the samples contained Ti, O and C. The Ti and O elements were assigned to TiO_2, and the O was also related with HA, whereas the C element was mainly related to adventitious hydrocarbon during the measurement. There were F and N elements detected on MS surface, which was associated with the residual fluoride and ammonium from the electrolyte. After annealing, the peaks of F or N disappeared on MS-450 and MS-550, because of the decomposition of the residues caused by calcination. After HA modification, the characteristic peaks of Ca and P elements appeared on the MS-HA, MS-450-HA and MS-550-HA samples. It is noteworthy that compared with MS, MS-HA had a lower concentration (~1.77 at%) of F element and negligible concentration (~0 at%) of N element, which were owing to the fact that the HA partially covered the TiO_2 surface and reduced the exposure area of oxides.

Table 1
The mean values (with ±1 SD error bars) of the microscale roughness (R_a) from different samples.

	R_a (μm)		R_a (μm)
MS	2.21 ± 0.13	MS-HA	2.22 ± 0.27
MS-450	2.16 ± 0.29	MS-450-HA	2.23 ± 0.39
MS-550	2.32 ± 0.25	MS-550-HA	2.39 ± 0.36

3.2. Surface wettability

Surface wettability was evaluated by sessile drop method and the contact angles of different liquids were listed in Table 3. Water droplet rapidly spread and wetted the micro/nanostructured surfaces of all the samples once added, and notably, the values of static contact angles were <5°, indicating the superhydrophilicity. As to diiodomethane, it is evident that the values of static contact angles were <5° as well for all the samples, revealing the superoleophilicity. Additionally, the similar results were obtained by measuring the contact angles of ethylene glycol and n-hexadecane. Hence, all the prepared samples were superamphiphilic, which were associated with the surface structures. The hierarchical micro/nanostructures on Ti surfaces greatly improved the surface roughness and capillary forces, inducing the rapid permeation of

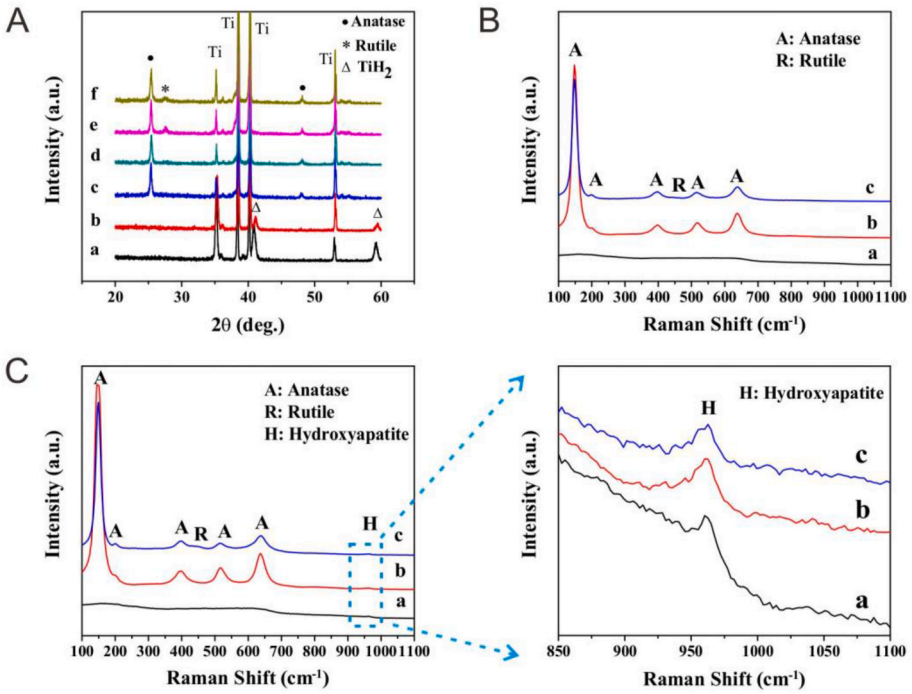

Fig. 3. (A) XRD patterns of different Ti samples: (a) MS, (b) MS-HA, (c) MS-450, (d) MS-450-HA, (e) MS-550 and (f) MS-550-HA. (B) Raman patterns of different Ti samples without HA modification: (a) MS, (b) MS-450, (C) MS-550. (C) Raman patterns of different Ti samples with HA modification: (a) MS-HA, (b) MS-450-HA, (c) MS-550-HA.

Table 2
The values of element concentrations according to the XPS results.

	Element (atom.%)						
	Ti	O	C	F	N	Ca	P
MS	23.29	46.99	25.46	3.32	0.94	–	–
MS-450	30.05	55.52	14.44	–	–	–	–
MS-550	29.83	55.06	15.11	–	–	–	–
MS-HA	4.63	55.81	16.02	1.77	–	12.21	9.56
MS-450-HA	2.65	57.18	15.33	–	–	13.71	11.14
MS-550-HA	4.80	56.81	14.67	–	–	13.33	10.39

Table 3
The values of contact angle of different Ti samples.

	Distilled water	Ethylene glycol	Diiodomethane	n-Hexadecane
	Contact angle (deg.°)			
MS	<5	<5	<5	<5
MS-HA	<5	<5	<5	<5
MS-450	<5	<5	<5	<5
MS-450-HA	<5	<5	<5	<5
MS-550	<5	<5	<5	<5
MS-550-HA	<5	<5	<5	<5

liquids into the porous structures [34].

3.3. Calcium ion release

The release profiles of Ca^{2+} ion was measured, as shown in Fig. 4. It is noted that Ca^{2+} ion was released much faster during the first 5 days for all the HA-modified samples, with the cumulative amounts of 21.45 mg/L, 36.25 mg/L, and 42.27 mg/L for MS-HA, MS-450-HA and MS-550-HA, respectilvely. After that, the steady release of Ca^{2+} ion was detected for

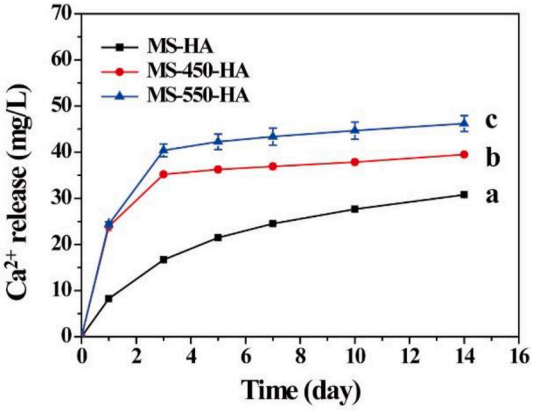

Fig. 4. The cumulative release of Ca^{2+} ion: (a) MS-HA, (b) MS-450-HA and (c) MS-550-HA.

all the groups, and by day 14, the amounts were 30.75 mg/L, 39.49 mg/L and 46.21 mg/L for MS-HA, MS-450-HA and MS-550-HA, respectively. The release kinetics of MS-450-HA and MS-550-HA were similar, where the daily release decreased faster with time than that of MS-HA.

3.4. Protein adsorption

Protein adsorption onto implant surfaces immediately occurs upon implantation of biomaterials and it significantly influences the cell adhesion and growth [2]. Therefore, to better mimic the material-protein interaction under cell culture condition, the different samples were immersed in α-MEM containing 10% FBS, and the amount of adsorbed proteins was measured. As shown in Fig. 5A, a similar amount of protein adsorption was discerned on all the samples without appreciable differences, although the average protein amounts adsorbed on MS, MS-550 and MS-550-HA were slightly higher than those on MS-HA, MS-450 and MS-450-HA.

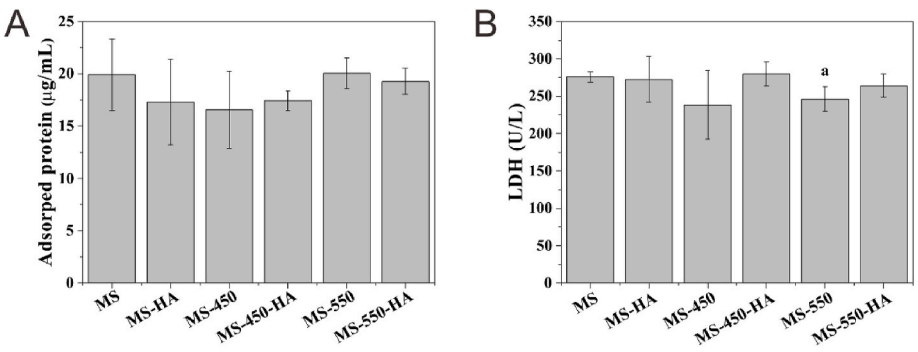

Fig. 5. (A) The amounts of protein adsorption on different Ti samples after immersion in cell culture medium containing 10% FBS. (B) The assay of LDH activity of the culture medium after 24-h incubation of cells on different Ti samples. [a]$p<0.05$ vs. MS.

3.5. Cytotoxicity assay

The release of lactate dehydrogenase (LDH) can disclose the cytotoxicity of the prepared samples towards the living cells. Fig. 5B presents the amount of LDH leakage of cells into the culture medium after incubation for 24 h. MS and MS-450 exhibited no appreciable difference in LDH activity between them although the latter showed a slightly lower value than the former. However, MS-550 displayed a significantly lower LDH activity than MS. After HA modification, the samples with HA achieved a maintained or slightly increased LDH activity than the respective samples without HA. It is clear that MS-450-HA and MS-550-HA marginally enhanced the LDH activity compared to MS-450 and MS-550, respectively, but the difference was negligible. The results demonstrate that the HA-modified micro/nanostructured surfaces did not cause the cytotoxicity towards the cells.

3.6. Cell morphology

The morphology of cells adhered to different samples after 24-h incubation was observed by SEM and fluorescence staining. As shown in Fig. 6, cells exhibited polygonal spreading on all the samples, and the filopodia as well as lamellipodia appeared to extend into the porous structures. It is interesting to note that cells on MS-450, MS-450-HA, MS-550 and MS-550-HA showed slightly more spread than cells on MS and MS-HA, indicating the better cell extensions on the former four samples. The similar adhesion morphology of cells on different samples was also discerned by fluorescence staining (Fig. S4). Previous reports have stated that surface topography of the substrates obviously influences cell adhesion and morphology [3,35]. The roughed Ti surface is able to distinctly regulate the cytoplasmic extensions and enable the cells with a much stronger adhesion to the substrates.

3.7. Cell proliferation

Cell proliferation on the different samples was measured by MTT assay, in which the OD value of formazan indirectly represents the viable cell number. As shown in Fig. 7A, MC3T3-E1 cells proliferated notably on all the samples during the culture period. After 1 day of culture, there

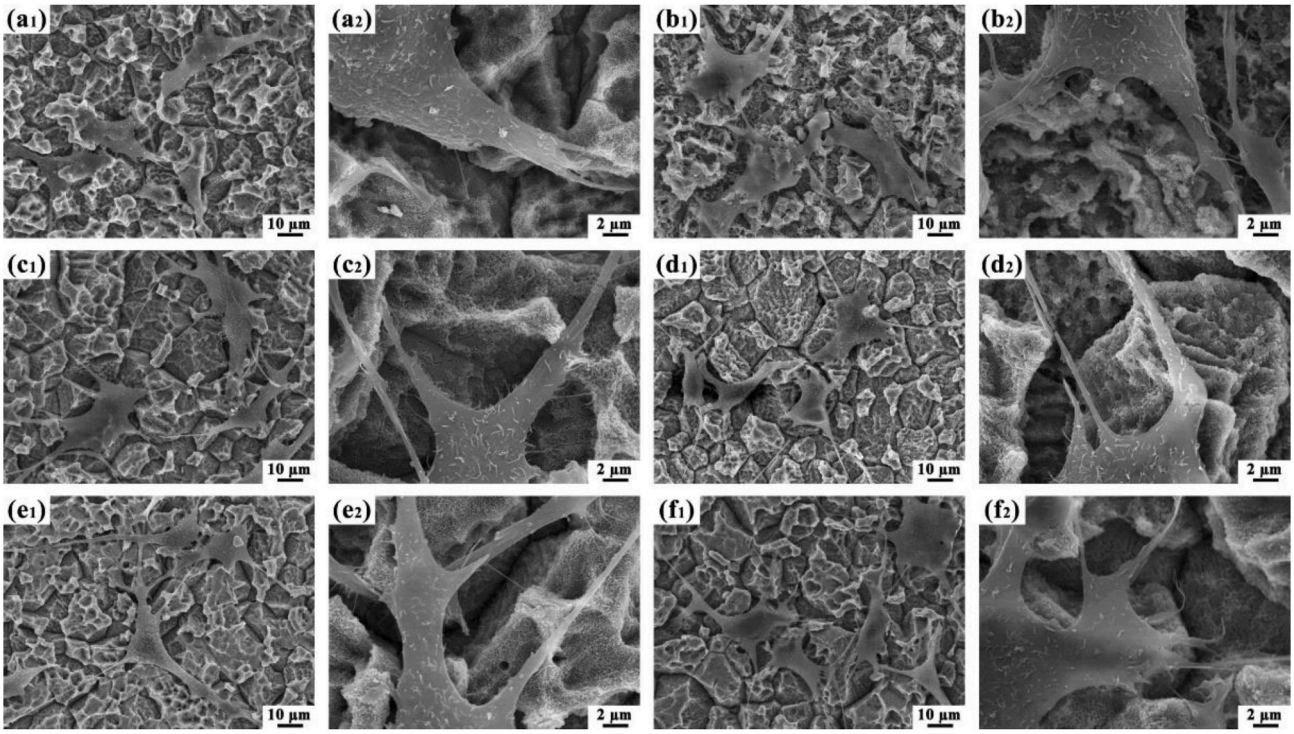

Fig. 6. Cell morphology after 24-h incubation on different Ti samples: (a) MS, (b) MS-HA, (c) MS-450, (d) MS-450-HA, (e) MS-550 and (f) MS-550-HA. Parts a_2–f_2 are high-magnification images of the samples in a_1–f_1, respectively.

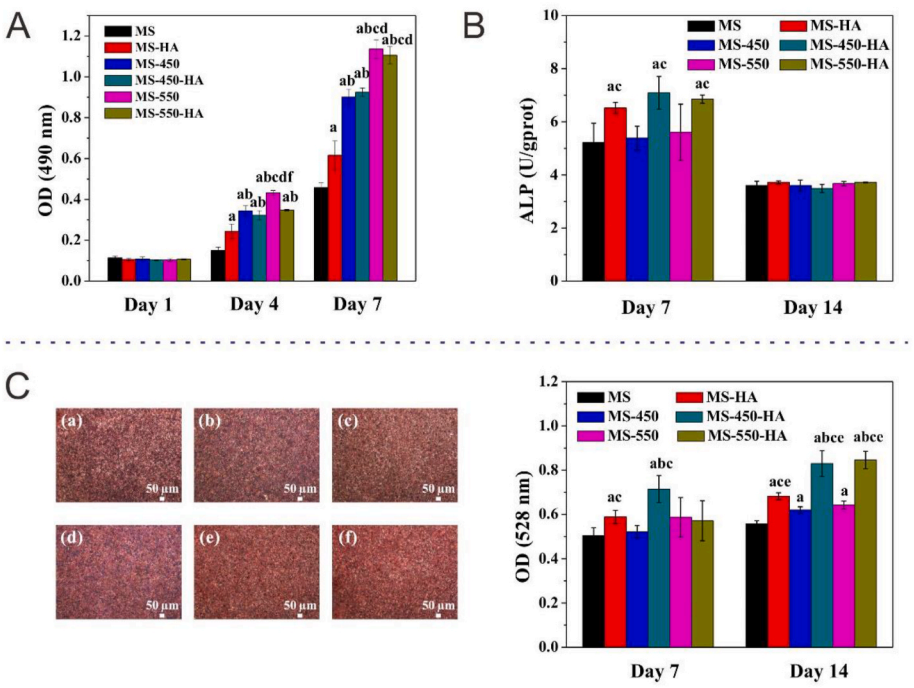

Fig. 7. (A) MTT assay of cells cultured on different Ti samples for 1, 4 and 7 days. (B) ALP activity of cells cultured on different Ti samples for 7 and 14 days. (C) Collagen production was evaluated by Sirius Red staining: optical images (left panel) of collagen secreted by cells after 7 days of culture on different Ti samples and the quantitative results (right panel) by colorimetric analysis. $^{a}p<0.05$ vs. MS, $^{b}p < 0.05$ vs. MS-HA, $^{c}p < 0.05$ vs. MS-450, $^{d}p < 0.05$ vs. MS-450-HA, $^{e}p < 0.05$ vs. MS-550, $^{f}p < 0.05$ vs. MS-550-HA.

was no distinct difference in cell numbers among all the groups. After 4 days of culture, the cell numbers on all the samples were significantly increased to varying degrees. The cells on the MS-450 and MS-550 were much more than cells on the MS. For the samples with HA modification, the cell number on the MS-HA was higher than that on the MS, however, the cell numbers on the MS-450-HA and MS-550-HA were slightly or significantly lower than on the MS-450 and MS-550, respectively. After 7 days of culture, the cells continued to proliferate. The highest cell numbers were observed on the MS-550 and MS-550-HA, followed by those on MS-450 and MS-450-HA, and MS displayed the lowest cell number. It is noted that similar cell numbers were obtained on MS-550 and MS-550-HA, MS-450 and MS-450-HA, respectively, but MS-HA showed much higher cell number than MS. In short, the cell numbers on different samples varies as MS-550-HA ≈ MS-550 > MS-450-HA ≈ MS-450 > MS-HA > MS.

Previous studies have indicated that the crystalline phase of TiO_2 significantly influences cell adhesion and proliferation, but no consistent conclusion has been achieved up to now (Table 4) [11–15,36]. For instance, Oh et al. found that the anatase TiO_2 nanotubes on Ti surface provided improved proliferation rate of MC3T3-E1 cells than the amorphous nanotubes [11]. Park et al. prepared amorphous or anatase TiO_2 nanotubes with different diameters, and observed that the proliferation rate of rat mesenchymal stem cells was somewhat higher on amorphous nanotubes than on anatase nanotubes [15]. Yu et al. showed that the proliferation trend of MC3T3-E1 cells on TiO_2 nanotubes with different crystalline phases was as follows, anatase/rutile > anatase > amorphous [12]. Bai et al. obtained the similar proliferation trend of MC3T3-E1 cells on anatase/rutile, anatase and amorphous TiO_2 nanotubes as the result of Yu et al. [36]. Cheng et al. noted that the anatase TiO_2 nanodot film presented a higher proliferation rate of NIH3T3 cells than the nanodots with anatase/rutile or rutile phase [37]. Our result indicates that the crystallized TiO_2 surfaces were able to improve the cell proliferation compared to the amorphous surface, especially the anatase/rutile surface displayed the highest cell proliferation rate, which was probably associated with the physicochemical properties of the prepared surfaces. Previous works have indicated that the protein conformation varies on TiO_2 surface with different crystalline phases [14,38,39]. For instance, Hong et al. observed that fibronectin (Fn) displayed a more favorable and active conformation, where more cell-adhesive epitopes were exposed, on the anatase TiO_2 nanodots with pre-adsorbed BSA than that on the amorphous nanodots, and thus resulted in better adhesion and proliferation of MC3T3-E1 cells [14]. Our data show that the

Table 4
Comparison of the main conclusion and differences in the reports on cell functions resulted from TiO_2 surface with different crystalline phases. Note: Am = amorphous, An = anatase, Ru = rutile, and TNTs = nanotubes.

	Morphology	Crystalline phase	Cell type	Main conclusion	
				Proliferation	Differentiation and mineralization
Oh et al. [11]	TNTs	Am, An	MC3T3-E1	An > Am	ALP: An > Am
Yu et al. [12]	TNTs	Am, An, An/Ru	MC3T3-E1	An/Ru > An > Am	Mineralization: An/Ru > An > Am
He et al. [13]	Flat film	Am, An, Ru	Primary rat osteoblasts	An > Ru ≈ Am	ALP: An > Ru ≈ Am
Hong et al. [14]	Nanodot film	Am, An	MC3T3-E1	An > Am	Mineralization: An > Am
Park et al. [15]	TNTs	Am, An	Rat mesenchymal stem cells	Proliferation rates were somewhat higher on Am than on An TNTs.	–
Bai et al. [36]	TNTs	Am, An, An/Ru	MC3T3-E1	An/Ru > An > Am	–
Cheng et al. [37]	Nanodot film	An, An/Ru, Ru	NIH3T3	An > An/Ru > Ru	–

calcination of the micro/nanostructured surfaces did not obviously change the surface morphology and wettability, but did significantly affect the proliferation of MC3T3-E1 cells, which was probably associated with the orientation and conformation of the adsorbed proteins on the prepared surfaces. It is generally accepted that the implant surfaces rapidly adsorb proteins (e.g., fibronectin, vitronectin and albumin) from the body fluids upon implantation, and the adsorbed states of proteins, such as the amount, types and conformation, greatly induce the cell adhesion and proliferation [40,41]. Among various proteins, Fn is the major cell-adhesive substrate and provides the epitopes for integrin binding [40]. The adsorbed state of Fn significantly impacts cell activities, including adhesion, migration, proliferation, differentiation and cytoskeletal organization [40,42]. Yang et al. observed that the conformation of adsorbed Fn or collagen on TiO_2 nanotubes was important for cell integrins to recognize the adhesive sites and in turn, the osteoblast viability was critically regulated [43]. Oh et al. [44] and Brammer et al. [45] also showed that the adsorbed nature of Fn or BSA on TiO_2 nanotube surface played a vital role in regulating the viability of human mesenchymal stem cells or MC3T3-E1 cells. Hence, it is reasonable to speculate that the various proliferation rates of MC3T3-E1 cells on micro/nanostructured surfaces with different crystalline phases are related to the orientation and conformation of adsorbed proteins.

In addition, the surface composition exerts an influence on the cell growth as well. Cooper et al. treated the TiO_2 grit-blasted Ti surface with HF, and observed that the residual fluoride (0.7–4 at%) enhanced the proliferation of human mesenchymal stem cells compared to the ones without fluoride modification [46]. Lamolle et al. etched the Ti surface with HF and noted that such modified surface was beneficial to MC3T3-E1 cell proliferation [47]. Similar positive effects of fluoride-modified Ti surfaces on proliferation of MG63 or MC3T3-E1 cells were discerned as well [48,49]. Moreover, Park et al. prepared TiO_2 nanotube arrays by anodization in 1 M H_3PO_4/0.30 M HF or 1 M H_3PO_4/0.12 HF solution to obtain amorphous samples with different amounts of residual fluoride ("high fluoride", 8.49 at% or "low fluoride", 2 at%) and the proliferation rates of rat mesenchymal stem cells on such samples were investigated [15]. Their result indicated that the different amounts of residual fluoride did not affect the cell proliferation trend even with the existences of N and P elements, while the high fluoride content may somewhat improve cell proliferation. According to the XPS data herein, 3.32 at% and 0.94% contents of F and N elements in MS may benefit cell proliferation. However, the cells on the calcined samples (MS-450 and MS-550) without residual F and N elements presented a much better proliferation rate than cells on MS, indicating that the crystalline phase of TiO_2 overrides the surface composition in cell proliferation.

As to the samples (MS-HA, MS-450-HA, MS-550-HA) with HA modification, MS-HA displayed a higher cell proliferation rate than MS, probably because the interaction between HA and amorphous TiO_2 induced the change in the adsorbed state of proteins. Cell proliferation rates on MS-450-HA and MS-550-HA were almost equal to the rates on MS-450 and MS-550, respectively, which is similar to the phenomena observed in others' reports [50–52]. Gu et al. [50], Nishio et al. [51], and Kim et al. [52], showed that Ti surfaces modified with HA did not improve cell proliferation rate compared with the ones without HA [50–52]. The reason for the above cell proliferation behaviors on HA-modified Ti surfaces are still unclear, which is probably associated with the microenvironment of HA-cell interactions [16].

3.8. Alkaline phosphatase activity

Alkaline phosphatase (ALP) activity, an early-stage differentiation marker, of osteoblast on different samples is displayed in Fig. 7B. After 7 days of culture, the values of ALP activity from MS, MS-450 and MS-550 were almost equal and interestingly, the values from MS-HA, MS-450-HA and MS-550-HA were similar as well, but the ALP activity from the latter groups were much higher than from the former groups. According to the quantitative comparisons, the ALP activity on MS-HA, MS-450-HA and MS-550-HA was increased by 24.9%, 31.6% and 22.2% compared with that of MS, MS-450 and MS-550, respectively, indicating HA was able to stimulate early differentiation of osteoblast. Although the ALP activity on MS-450-HA was slightly higher than that on MS-HA and MS-550-HA, the differences among the groups were negligible. After 14 days of culture, the ALP activity on all the samples was significantly reduced when compared to that at day 7, and notably, a similar level was observed among all the samples. The decrease trend of ALP activity is probably attributed to cells entering late-stage differentiation.

3.9. Collagen secretion

The secreted collagen on different samples was quantified by Sirius Red staining. As shown in Fig. 7C, after 7 days of culture, all the samples presented dark red and no obvious difference in color was observed under the optical microscope, indicating dense collagen products deposited on them. According to the quantitative analysis, the collagen products on MS, MS-450 and MS-550 were almost equal and no significant differences were observed among them. However, the collagen products on the HA-modified samples were maintained or enhanced compared with the samples without HA modification. It is clear that MS-HA and MS-450-HA displayed much more collagen products than MS and MS-450, respectively, but no significant difference was discerned between MS-550 and MS-550-HA. As the culture time prolonged to 14 days, the collagen products on all the samples were increased to varying degrees, and the HA-modified samples presented a higher increasing extent than the ones without HA. The collagen products on MS-HA, MS-450-HA and MS-550-HA were increased by 22.2%, 33.9% and 31.6% compared with MS, MS-450 and MS-550, respectively, and simultaneously, the most and similar collagen products were observed on MS-450-HA and MS-550-HA. Among the samples without HA, MS-450 and MS-550 displayed more collagen products than MS. In short, the collagen deposition on different samples varies as MS-550-HA $\approx$ MS-450-HA $>$ MS-HA $>$ MS-550 $\approx$ MS-450 $>$ MS.

3.10. Extracellular matrix mineralization

The extracellular matrix mineralization was examined by SEM analysis and calcium content test. As shown in Fig. 8A, cells rich in collagen fibers spread closely on all the samples and the morphology presented polygonal, indicating the favorable growth state of cells [53]. Based on the quantitative analysis (Fig. 8B), MS-550 showed a slightly higher calcium content than MS and MS-450, but the difference was not significant. It is clear that, after HA addition, the ones with HA achieved a slightly or significantly higher amount of calcium than the respective ones without HA. Collectively, the amount of calcium deposited on MS-450-HA and MS-550-HA was similar, which was much higher than that on MS, MS-HA or MS-450. Additionally, the calcium content on MS-450-HA was obviously higher than that on MS-450; in contrast, the amount on MS-HA and MS-550-HA was slightly higher than that on MS and MS-550, respectively, but without significant differences.

According to the results of ALP activity, collagen secretion and extracellular matrix mineralization, it is noteworthy that MS, MS-450 and MS-550 did not show any significant differences in cell differentiation and extracellular matrix mineralization. The results herein differed from some others' studies [11–13]. For instance, Oh et al. observed that ALP activity of MC3T3-E1 cells on anatase TiO_2 nanotubes was higher than that on amorphous nanotubes [11]. Yu et al. perceived that the mineralization trend of MC3T3-E1 cells on nanotubes with different crystalline phases was as follows, anatase/rutile $>$ anatase $>$ amorphous [12]. However, no obvious differences among anatase/rutile, anatase and amorphous groups were discerned in this study, which is probably due to the fact that the hierarchical micro/nanostructures outweigh other factors (e.g., crystalline phase and chemical composition) in affecting cell differentiation and extracellular matrix mineralization.

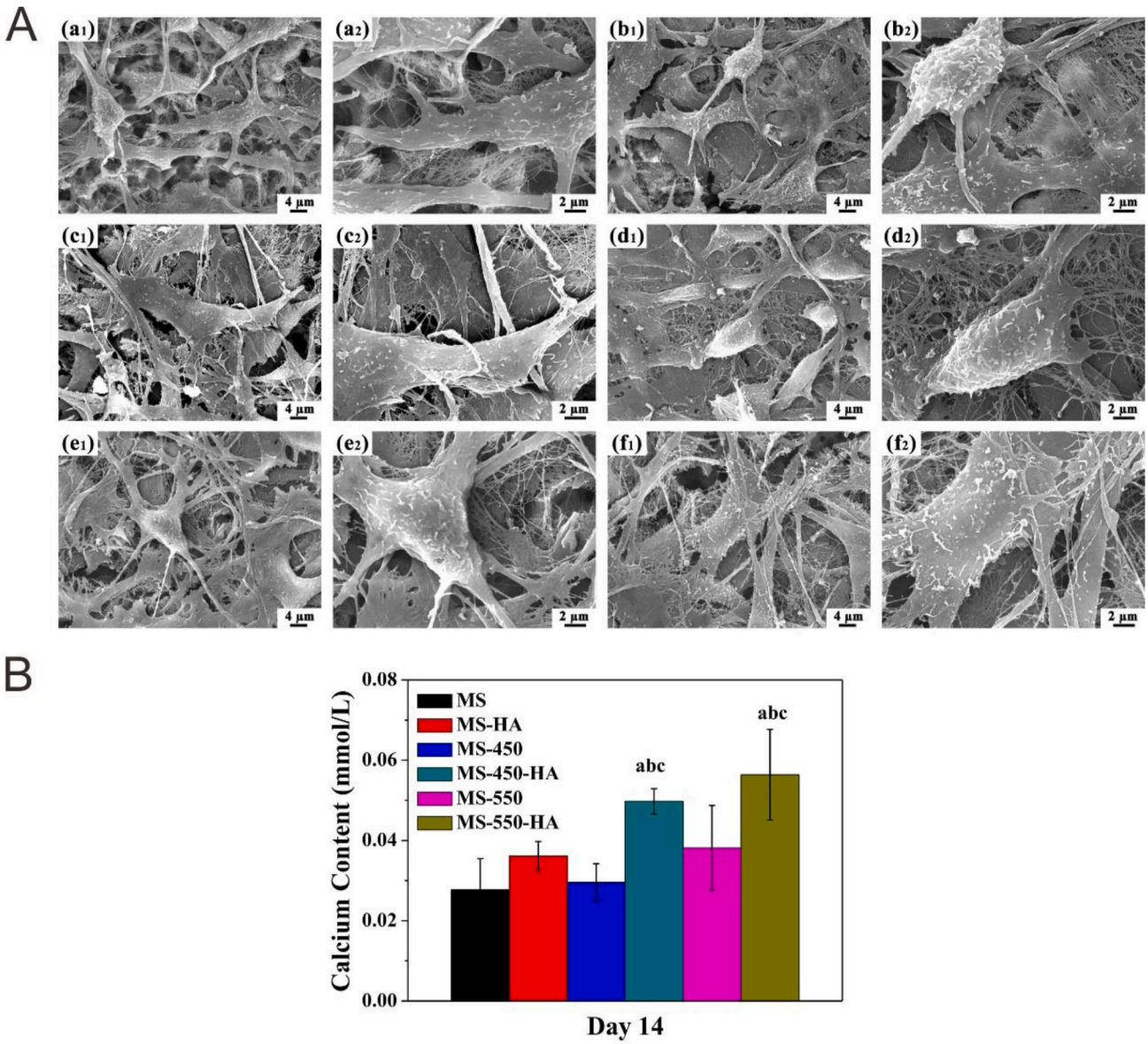

Fig. 8. (A) SEM images of cell morphology on different Ti samples after 14 days of incubation: (a) MS, (b) MS-HA, (c) MS-450, (d) MS-450-HA, (e) MS-550 and (f) MS-550-HA. Parts a_2–f_2 are high-magnification images of the samples in a_1–f_1, respectively. (B) The amounts of calcium deposited on different Ti samples by cells after 14 days of incubation. $^{a}p<0.05$ vs. MS, $^{b}p < 0.05$ vs. MS-HA, $^{c}p < 0.05$ vs. MS-450.

Previous works have shown that the microscale structures stimulated cell differentiation and extracellular matrix mineralization [54–57], and the addition of nanoscale features to the microscale features was able to improve the cell differentiation and mineralization compared to the microstructured surfaces [4–6]. Our early study has also noted that the differentiation and extracellular matrix mineralization of MC3T3-E1 cells was greatly enhanced on MS-450 [58]. In addition, the improved wettability of the microscale or a combined micro- and nanoscale surface features tends to favor osteoblast differentiation and maturation [59]. Therefore, it is probable that the hierarchically micro/nanoscale structures on all the prepared samples critically improve cell differentiation and extracellular matrix mineralization compared to crystalline phases of TiO_2 as well as surface chemical composition, and the enhanced hydrophilicity may be also beneficial.

As to the samples with HA modification, MS-HA, MS-450-HA and MS-550-HA presented much higher cell differentiation and extracellular matrix mineralization than the ones without HA. It is generally accepted that HA is bioactive and osteoconductive [19,20,60,61]. Previous studies have confirmed that HA-modified Ti surfaces can promote cell differentiation and maturation in vitro [50–52,62], and also, HA-deposited implants were able to induce bone ingrowth at the bone-implant interface without isolation by fibrous tissue layer in vivo [20,63–66]. Although the detailed mechanism is still under exploration, the superior bioactivity and osteoconductivity of HA are related to its physicochemical properties, such as composition, morphology and geometry [16,20,67]. Moreover, the release of calcium and phosphate ions from HA into the cell-material microenvironment probably enhanced the ALP activity and extracellular matrix mineralization [16,67]. Ca^{2+} ion plays an important role in modulating cellular functions through specific sites and receptors, including calcium-related proteins (e.g., pancreatic stone protein), extracellular matrix proteins (e.g., fibulin) and gene-associated signaling (e.g., SOX9) [68]. The uptake and regulation of Ca^{2+} ion may lead to activation of signal transduction pathways, favoring osteoblast differentiation. PO_4^{3-} ion was also considered as a signaling molecule, which probably induced the temporal coordination of the differentiation process by modulating expression and regulation of multiple factors [69]. In short, the released ions may not only facilitate intracellular signaling pathways, but also benefit

extracellular mineral deposition.

In addition, the previous study has reported that osteoblasts can synthesize and secrete mineralization-related proteins, such as osteopontin, bone sialoprotein and osteocalcin [70]. These proteins are able to bind to hydroxyapatite and, in turn, the binding and accumulation of mineralization-related proteins contribute to the maturation and deposition of extracellular matrix. Hence, the better performance of HA-modified samples in improving cell differentiation and maturation is probably associated with the unique physiological functions and bioactivity of HA. Moreover, there is no obvious difference in ALP activity among MS-HA, MS-450-HA and MS-550-HA, but the collagen production and calcium deposition on MS-450-HA and MS-550-HA are higher than on MS-HA, which probably is resulted from the combined effects of crystalline phase and HA on cell functions. Briefly, the early differentiation and extracellular matrix mineralization of osteoblasts on different samples vary as MS-550-HA ≈ MS-450-HA > MS-HA > MS-550 ≈ MS-450 ≈ MS.

In a word, it is indicated that micro/nanostructured surfaces (MS, MS-450 and MS-550) with different crystalline phases can significantly affect the proliferation of osteoblasts, but cannot obviously influence the differentiation and mineralization. After HA addition, the HA-modified micro/nanostructured surfaces (MS-HA, MS-450-HA and MS-550-HA) are able to considerably improve the differentiation and mineralization of osteoblasts but without compromising the proliferation trend of osteoblasts on MS, MS-450 and MS-550. Therefore, our results suggest that the combination of micro/nanostructured surfaces possessing proper crystalline phase with bioactive HA composition may markedly improve the bioactivity and biocompatibility of Ti implants, thereby enhancing the osseointegration in vivo.

4. Conclusions

In this study, the micro/nanostructured surfaces with different crystalline phases (amorphous, anatase and anatase/rutile) were constructed on medical Ti substrates by combined treatments of acid etching, anodization and calcination. Then an ultrathin film of nanoscale HA was immobilized onto the above surfaces by a spin-assisted layer-by-layer technique to form HA-modified micro/nanostructured surfaces. All of the samples displayed similar surface morphology and wettability (superamphiphilic). It was demonstrated that the surface crystalline phase was able to offer a significant impact on the proliferation trend of MC3T3-E1 cells and the anatase/rutile mixture achieved the highest proliferation rate, followed by the anatase, but it cannot appreciably influence the trend of cell differentiation and mineralization. However, the nanoscale HA-modified micro/nanostructured surfaces with different crystalline phases led to the significantly improved effects on cell differentiation and extracellular matrix mineralization, but the proliferation trend of cells was comparable to that on the ones without HA deposition. The study herein extends the systematic understanding towards the relationship among crystalline phase, HA modification and osteoblast response, and thus provides a promising strategy on improving the osseointegration of Ti implants.

CRediT authorship contribution statement

Pinliang Jiang: Conceptualization, Investigation, Writing - original draft. **Yanmei Zhang:** Investigation. **Ren Hu:** Visualization, Writing - review & editing. **Xiankuan Wang:** Investigation. **Yuekun Lai:** Writing - review & editing. **Gang Rui:** Writing - review & editing. **Changjian Lin:** Conceptualization, Supervision, Writing - review & editing.

Declaration of competing interest

The authors declare no conflict of interest.

Acknowledgements

This work was financially supported by the Ministry of Science and Technology of China (grant No. 2016YFC1100300), and the National Natural Science Foundation of China (grant No. 21773199, 51571169).

Appendix A. Supplementary data

Supplementary data to this article can be found online at https://doi.org/10.1016/j.bioactmat.2020.10.006.

References

[1] S. Bauer, P. Schmuki, K. von der Mark, J. Park, Engineering biocompatible implant surfaces: Part I: materials and surfaces, Prog. Mater. Sci. 58 (3) (2013) 261–326.
[2] C. Stewart, B. Akhavan, S.G. Wise, M.M.M. Bilek, A review of biomimetic surface functionalization for bone-integrating orthopedic implants: mechanisms, current approaches, and future directions, Prog. Mater. Sci. 106 (2019) 100588.
[3] Y. Li, Y. Xiao, C. Liu, The horizon of materiobiology: a perspective on material-guided cell behaviors and tissue engineering, Chem. Rev. 117 (5) (2017) 4376–4421, 2017.
[4] K. Kubo, N. Tsukimura, F. Iwasa, T. Ueno, L. Saruwatari, H. Aita, W.A. Chiou, T. Ogawa, Cellular behavior on TiO_2 nanonodular structures in a micro-to-nanoscale hierarchy model, Biomaterials 30 (29) (2009) 5319–5329.
[5] L. Zhao, S. Mei, P.K. Chu, Y. Zhang, Z. Wu, The influence of hierarchical hybrid micro/nano-textured titanium surface with titania nanotubes on osteoblast functions, Biomaterials 31 (19) (2010) 5072–5082.
[6] R.A. Gittens, T. McLachlan, R. Olivares-Navarrete, Y. Cai, S. Berner, R. Tannenbaum, Z. Schwartz, K.H. Sandhage, B.D. Boyan, The effects of combined micron-/submicron-scale surface roughness and nanoscale features on cell proliferation and differentiation, Biomaterials 32 (13) (2011) 3395–3403.
[7] R.A. Gittens, R. Olivares-Navarrete, A. Cheng, D.M. Anderson, T. McLachlan, I. Stephan, J. Geis-Gerstorfer, K.H. Sandhage, A.G. Fedorov, F. Rupp, B.D. Boyan, R. Tannenbaum, Z. Schwartz, The roles of titanium surface micro/nanotopography and wettability on the differential response of human osteoblast lineage cells, Acta Biomater. 9 (4) (2013) 6268–6277.
[8] Q. Liu, W. Wang, L. Zhang, L. Zhao, W. Song, X. Duan, Y. Zhang, Involvement of N-cadherin/β-catenin interaction in the micro/nanotopography induced indirect mechanotransduction, Biomaterials 35 (24) (2014) 6206–6218.
[9] E.G. Long, M. Buluk, M.B. Gallagher, J.M. Schneider, J.L. Brown, Human mesenchymal stem cell morphology, migration, and differentiation on micro and nano-textured titanium, Bioactive Materials 4 (2019) 249–255.
[10] A. Cheng, W.B. Goodwin, B.M. deGlee, R.A. Gittens, J.P. Vernon, S.L. Hyzy, Z. Schwartz, K.H. Sandhage, B.D. Boyan, Surface modification of bulk titanium substrates for biomedical applications via low-temperature microwave hydrothermal oxidation, J. Biomed. Mater. Res. Part A 106A (3) (2018) 782–796.
[11] S. Oh, C. Daraio, L.H. Chen, T.R. Pisanic, R.R. Finones, S. Jin, Significantly accelerated osteoblast cell growth on aligned TiO_2 nanotubes, J. Biomed. Mater. Res. Part A 78A (1) (2006) 97–103.
[12] W.Q. Yu, Y.L. Zhang, X.Q. Jiang, F.Q. Zhang, In vitro behavior of MC3T3-E1 preosteoblast with different annealing temperature titania nanotubes, Oral Dis. 16 (7) (2010) 624–630.
[13] J. He, W. Zhou, X.J. Zhou, X.X. Zhong, X.L. Zhang, P.B. Wan, B.S. Zhu, W.T. Chen, The anatase phase of nanotopography titania plays an important role on osteoblast cell morphology and proliferation, J. Mater. Sci. Mater. Med. 19 (11) (2008) 3465–3472.
[14] Y. Hong, M. Yu, J. Lin, K. Cheng, W. Weng, H. Wang, Surface hydroxyl groups direct cellular response on amorphous and anatase TiO_2 nanodots, Colloids Surf. B Biointerfaces 123 (2014) 68–74.
[15] J. Park, S. Bauer, P. Schmuki, K. von der Mark, Narrow window in nanoscale dependent activation of endothelial cell growth and differentiation on TiO_2 vanotube surfaces, Nano Lett. 9 (9) (2009) 3157–3164.
[16] R.A. Surmenev, M.A. Surmeneva, A.A. Ivanova, Significance of calcium phosphate coatings for the enhancement of new bone osteogenesis – a review, Acta Biomater. 10 (2) (2014) 557–579.
[17] Y. Su, I. Cockerill, Y. Zheng, L. Tang, Y.-X. Qin, D. Zhu, Biofunctionalization of metallic implants by calcium phosphate coatings, Bioactive Materials 4 (2019) 196–206.
[18] S.A. Mali, K.C. Nune, R.D.K. Misra, Biomimetic nanostructured hydroxyapatite coatings on metallic implant materials, Mater. Technol. 31 (13) (2016) 782–790.
[19] Y. Hong, H. Fan, B. Li, B. Guo, M. Liu, X. Zhang, Fabrication, biological effects, and medical applications of calcium phosphate nanoceramics, Mater. Sci. Eng. R Rep. 70 (3) (2010) 225–242.
[20] R.Z. LeGeros, Calcium phosphate-based osteoinductive materials, Chem. Rev. 108 (11) (2008) 4742–4753.
[21] C.M. Xie, X. Lu, K.F. Wang, F.Z. Meng, O. Jiang, H.P. Zhang, W. Zhi, L.M. Fang, Silver nanoparticles and growth factors incorporated hydroxyapatite coatings on metallic implant surfaces for enhancement of osteoinductivity and antibacterial properties, ACS Appl. Mater. Interfaces 6 (11) (2014) 8580–8589.
[22] U. Ripamonti, L.C. Roden, L.F. Renton, Osteoinductive hydroxyapatite-coated titanium implants, Biomaterials 33 (15) (2012) 3813–3823.

[23] W. Chen, X. Shen, Y. Hu, K. Xu, Q. Ran, Y. Yu, L. Dai, Z. Yuan, L. Huang, T. Shen, K. Cai, Surface functionalization of titanium implants with chitosan-catechol conjugate for suppression of ROS-induced cells damage and improvement of osteogenesis, Biomaterials 114 (2017) 82–96.
[24] A. Civantos, E. Martínez-Campos, V. Ramos, C. Elvira, A. Gallardo, A. Abarrategi, Titanium coatings and surface modifications: toward clinically useful bioactive implants, ACS Biomater. Sci. Eng. 3 (7) (2017) 1245–1261.
[25] R.B. Heimann, Plasma-sprayed hydroxylapatite-based coatings: chemical, mechanical, microstructural, and biomedical properties, J. Therm. Spray Technol. 25 (5) (2016) 827–850.
[26] L.J. Raggatt, N.C. Partridge, Cellular and molecular mechanisms of bone remodeling, J. Biol. Chem. 285 (33) (2010) 25103–25108.
[27] E. Landi, A. Tampieri, G. Celotti, S. Sprio, Densification behaviour and mechanisms of synthetic hydroxyapatites, J. Eur. Ceram. Soc. 20 (14) (2000) 2377–2387.
[28] O.K. Varghese, D. Gong, M. Paulose, C.A. Grimes, E.C. Dickey, Crystallization and high-temperature structural stability of titanium oxide nanotube arrays, J. Mater. Res. 18 (1) (2003) 156–165.
[29] A. Stoch, A. Brożek, S. Błażewicz, W. Jastrzębski, J. Stoch, A. Adamczyk, I. Rój, FTIR study of electrochemically deposited hydroxyapatite coatings on carbon materials, J. Mol. Struct. 651–653 (2003) 389–396.
[30] G. Xu, I.A. Aksay, J.T. Groves, Continuous crystalline carbonate apatite thin films. A biomimetic approach, J. Am. Chem. Soc. 123 (10) (2001) 2196–2203.
[31] L. Gao, B. Feng, J. Wang, X. Lu, D. Liu, S. Qu, J. Weng, Micro/nanostructural porous surface on titanium and bioactivity, J. Biomed. Mater. Res. B Appl. Biomater. 89B (2) (2009) 335–341.
[32] S. Sahoo, A.K. Arora, V. Sridharan, Raman line shapes of optical phonons of different symmetries in anatase TiO_2 nanocrystals, J. Phys. Chem. C 113 (39) (2009) 16927–16933.
[33] M. Kazanci, P. Fratzl, K. Klaushofer, E.P. Paschalis, Complementary information on in vitro conversion of amorphous (precursor) calcium phosphate to hydroxyapatite from Raman microspectroscopy and wide-angle X-Ray scattering, Calcif. Tissue Int. 79 (5) (2006) 354–359.
[34] K. Liu, M. Cao, A. Fujishima, L. Jiang, Bio-inspired titanium dioxide materials with special wettability and their applications, Chem. Rev. 114 (19) (2014) 10044–10094.
[35] H. Amani, H. Arzaghi, M. Bayandori, A.S. Dezfuli, H. Pazoki-Toroudi, A. Shafiee, L. Moradi, Controlling cell behavior through the design of biomaterial surfaces: a focus on surface modification techniques, Advanced Materials Interfaces 6 (13) (2019) 1900572.
[36] Y. Bai, I.S. Park, H.H. Park, M.H. Lee, T.S. Bae, W. Duncan, M. Swain, The effect of annealing temperatures on surface properties, hydroxyapatite growth and cell behaviors of TiO_2 nanotubes, Surf. Interface Anal. 43 (6) (2011) 998–1005.
[37] K. Cheng, Y. Sun, H. Wan, X. Wang, W. Weng, J. Lin, H. Wang, Improved light-induced cell detachment on rutile TiO_2 nanodot films, Acta Biomater. 26 (2015) 347–354.
[38] J. Sund, H. Alenius, M. Vippola, K. Savolainen, A. Puustinen, Proteomic characterization of engineered nanomaterial–protein interactions in relation to surface reactivity, ACS Nano 5 (6) (2011) 4300–4309.
[39] S. Köppen, O. Bronkalla, W. Langel, Adsorption configurations and energies of amino acids on anatase and rutile surfaces, J. Phys. Chem. C 112 (35) (2008) 13600–13606.
[40] K. von der Mark, J. Park, Engineering biocompatible implant surfaces Part II: cellular recognition of biomaterial surfaces: lessons from cell-matrix interactions, Prog. Mater. Sci. 58 (3) (2013) 327–381.
[41] I. Degasne, M.F. Baslé, V. Demais, G. Huré, M. Lesourd, B. Grolleau, L. Mercier, D. Chappard, Effects of roughness, fibronectin and vitronectin on attachment, spreading, and proliferation of human osteoblast-like cells (Saos-2) on titanium surfaces, Calcif. Tissue Int. 64 (6) (1999) 499–507.
[42] E. Cukierman, R. Pankov, K.M. Yamada, Cell interactions with three-dimensional matrices, Curr. Opin. Cell Biol. 14 (5) (2002) 633–639.
[43] W. Yang, X. Xi, X. Shen, P. Liu, Y. Hu, K. Cai, Titania nanotubes dimensions-dependent protein adsorption and its effect on the growth of osteoblasts, J. Biomed. Mater. Res. Part A 102A (10) (2014) 3598–3608.
[44] S. Oh, K.S. Brammer, Y.S.J. Li, D. Teng, A.J. Engler, S. Chien, S. Jin, Stem cell fate dictated solely by altered nanotube dimension, Proc. Natl. Acad. Sci. Unit. States Am. 106 (7) (2009) 2130–2135.
[45] K.S. Brammer, S. Oh, C.J. Cobb, L.M. Bjursten, H.v.d. Heyde, S. Jin, Improved bone-forming functionality on diameter-controlled TiO_2 nanotube surface, Acta Biomater. 5 (8) (2009) 3215–3223.
[46] L.F. Cooper, Y. Zhou, J. Takebe, J. Guo, A. Abron, A. Holmén, J.E. Ellingsen, Fluoride modification effects on osteoblast behavior and bone formation at TiO_2 grit-blasted c.p. titanium endosseous implants, Biomaterials 27 (6) (2006) 926–936.
[47] S.F. Lamolle, M. Monjo, M. Rubert, H.J. Haugen, S.P. Lyngstadaas, J.E. Ellingsen, The effect of hydrofluoric acid treatment of titanium surface on nanostructural and chemical changes and the growth of MC3T3-E1 cells, Biomaterials 30 (5) (2009) 736–742.
[48] H.Y. Liu, X.J. Wang, L.P. Wang, F.Y. Lei, X.F. Wang, H.J. Ai, Effect of fluoride-ion implantation on the biocompatibility of titanium for dental applications, Appl. Surf. Sci. 254 (20) (2008) 6305–6312.
[49] S.E. Kim, J.H. Lim, S.C. Lee, S.-C. Nam, H.G. Kang, J. Choi, Anodically nanostructured titanium oxides for implant applications, Electrochim. Acta 53 (14) (2008) 4846–4851.
[50] Y.X. Gu, J. Du, J.M. Zhao, M.S. Si, J.J. Mo, H.C. Lai, Characterization and preosteoblastic behavior of hydroxyapatite-deposited nanotube surface of titanium prepared by anodization coupled with alternative immersion method, J. Biomed. Mater. Res. B Appl. Biomater. 100B (8) (2012) 2122–2130.
[51] K. Nishio, M. Neo, H. Akiyama, S. Nishiguchi, H.M. Kim, T. Kokubo, T. Nakamura, The effect of alkali- and heat-treated titanium and apatite-formed titanium on osteoblastic differentiation of bone marrow cells, J. Biomed. Mater. Res. 52 (4) (2000) 652–661.
[52] D.Y. Kim, M. Kim, H.E. Kim, Y.H. Koh, H.W. Kim, J.H. Jang, Formation of hydroxyapatite within porous TiO_2 layer by micro-arc oxidation coupled with electrophoretic deposition, Acta Biomater. 5 (6) (2009) 2196–2205.
[53] W.W. Thein-Han, R.D.K. Misra, Biomimetic chitosan–nanohydroxyapatite composite scaffolds for bone tissue engineering, Acta Biomater. 5 (4) (2009) 1182–1197.
[54] M.J. Kim, C.W. Kim, Y.J. Lim, S.J. Heo, Microrough titanium surface affects biologic response in MG63 osteoblast-like cells, J. Biomed. Mater. Res. 79A (4) (2006) 1023–1032.
[55] O. Zinger, G. Zhao, Z. Schwartz, J. Simpson, M. Wieland, D. Landolt, B. Boyan, Differential regulation of osteoblasts by substrate microstructural features, Biomaterials 26 (14) (2005) 1837–1847.
[56] K. Takeuchi, L. Saruwatari, H.K. Nakamura, J.M. Yang, T. Ogawa, Enhanced intrinsic biomechanical properties of osteoblastic mineralized tissue on roughened titanium surface, J. Biomed. Mater. Res. Part A 72A (3) (2005) 296–305.
[57] Z. Schwartz, R. Olivares-Navarrete, M. Wieland, D.L. Cochran, B.D. Boyan, Mechanisms regulating increased production of osteoprotegerin by osteoblasts cultured on microstructured titanium surfaces, Biomaterials 30 (20) (2009) 3390–3396.
[58] P. Jiang, J. Liang, R. Song, Y. Zhang, L. Ren, L. Zhang, P. Tang, C. Lin, Effect of octacalcium-phosphate-modified micro/nanostructured titania surfaces on osteoblast response, ACS Appl. Mater. Interfaces 7 (26) (2015) 14384–14396.
[59] R.A. Gittens, L. Scheideler, F. Rupp, S.L. Hyzy, J. Geis-Gerstorfer, Z. Schwartz, B. D. Boyan, A review on the wettability of dental implant surfaces II: biological and clinical aspects, Acta Biomater. 10 (7) (2014) 2907–2918.
[60] W.W. Thein-Han, R.D.K. Misra, Three-dimensional chitosan-nanohydroxyapatite composite scaffolds for bone tissue engineering, JOM-J. Miner. Met. Mater. Soc. 61 (9) (2009) 41–44.
[61] A. Kumar, K.C. Nune, R.D.K. Misra, Biological functionality of extracellular matrix-ornamented three-dimensional printed hydroxyapatite scaffolds, J. Biomed. Mater. Res. Part A 104A (6) (2016) 1343–1351.
[62] J. Yang, K. Zhang, K. Que, S. Hou, Z. Chen, Y. Li, Y. Wang, Y. Song, B. Guan, W. Zhang, D. Zhu, C. Li, D. Wang, P. Geng, X. Zhang, Surface modification of titanium with hydroxyapatite layer induced by phase-transited lysozyme coating, Mater. Sci. Eng. C 92 (2018) 206–215.
[63] J.W.M. Vehof, P.H.M. Spauwen, J.A. Jansen, Bone formation in calcium-phosphate-coated titanium mesh, Biomaterials 21 (19) (2000) 2003–2009.
[64] W. Xue, S. Tao, X. Liu, X. Zheng, C. Ding, In vivo evaluation of plasma sprayed hydroxyapatite coatings having different crystallinity, Biomaterials 25 (3) (2004) 415–421.
[65] A. Thorfve, C. Lindahl, W. Xia, K. Igawa, A. Lindahl, P. Thomsen, A. Palmquist, P. Tengvall, Hydroxyapatite coating affects the Wnt signaling pathway during peri-implant healing in vivo, Acta Biomater. 10 (3) (2014) 1451–1462.
[66] Y. Li, W. Yang, X. Li, X. Zhang, C. Wang, X. Meng, Y. Pei, X. Fan, P. Lan, C. Wang, X. Li, Z. Guo, Improving osteointegration and osteogenesis of three-dimensional porous Ti6Al4V scaffolds by polydopamine-assisted biomimetic hydroxyapatite coating, ACS Appl. Mater. Interfaces 7 (10) (2015) 5715–5724.
[67] D. Xiao, J. Zhang, C. Zhang, D. Barbieri, H. Yuan, L. Moroni, G. Feng, The role of calcium phosphate surface structure in osteogenesis and the mechanisms involved, Acta Biomater. 106 (2020) 22–33.
[68] J.H. Song, J.H. Kim, S. Park, W. Kang, H.W. Kim, H.E. Kim, J.H. Jang, Signaling responses of osteoblast cells to hydroxyapatite: the activation of ERK and SOX9, J. Bone Miner. Metabol. 26 (2) (2008) 138–142.
[69] G.R. Beck Jr., Inorganic phosphate as a signaling molecule in osteoblast differentiation, J. Cell. Biochem. 90 (2) (2003) 234–243.
[70] J.B. Lian, G.S. Stein, Concepts of osteoblast growth and differentiation: basis for modulation of bone cell development and tissue formation, Crit. Rev. Oral Biol. Med. 3 (3) (1992) 269–305.